Proceedings of the 10th Brazilian Congress of Thermal Sciences and Engineering -- ENCIT 2004
Braz. Soc. of Mechanical Sciences and Engineering -- ABCM, Rio de Janeiro, Brazil, Nov. 29 -- Dec. 03, 2004

Paper CIT04-0801

SURFACE TEMPERATURE EFFECTS IN LOW-DENSITY FLOW OVER FLAT-NOSE BODIES AT HYPERSONIC SPEED. PART III: SHOCK WAVE STRUCTURE

Wilson F. N. Santos
National Institute for Space Research
Combustion and Propulsion Laboratory
12630-000 Cachoeira Paulista, SP, Brazil
wilson@lcp.inpe.br

Abstract. *Computations using the Direct Simulation Monte Carlo (DSMC) method are presented for hypersonic flow over flat-nose leading edges. The primary aim of this paper is to examine the effect of the body surface temperature on the shock wave structure. The sensitivity of shock wave shape, shock standoff distance, and shock thickness to wall temperature variations is calculated by using a model that classifies the molecules in three distinct classes, i.e., "undisturbed freestream", "reflected from the boundary" and "scattered", i.e., molecules that had been indirectly affected by the presence of the leading edge. The analysis shows significant differences on the shock wave structure due to variations on the body surface temperature. It was found that the flat-nose leading edges provided smaller shock wave standoff distance and shock wave thickness, compared to the corresponding circular cylinder that generated the flat-nose bodies.*

Keywords. *DSMC, hypersonic flow, rarefied flow, blunt leading edge, shock standoff distance, shock wave thickness.*

1. Introduction

The successful design of high-lift, low-drag hypersonic configurations will depend on the ability to incorporate relatively sharp leading edges that combine good aerodynamic properties with acceptable heating rates. Certain configurations, such as hypersonic waveriders (Nonweiler, 1959), are designed analytically with infinitely sharp leading edge for shock wave attachment. However, for practical applications, these sharp leading edges must be blunted for heat transfer, manufacturing, and handling concerns, with associated departures from ideal performance. Typically, a round leading edge (circular cylinder) with constant radius of curvature near the stagnation point has been chosen. Nevertheless, shock detachment distance on a cylinder, with associated leakage, scales with the radius of curvature. Certain classes of non-circular shapes may provide the required bluntness with smaller shock separation than round leading edges, thus allowing manufacturing, and ultimately heating control, with reduced aerodynamic losses.

A typical blunt body, composed of a flat nose followed by a highly curved, but for the most part slightly inclined afterbody surface, may provide the required bluntness for heat transfer, manufacturing and handling concerns with reduced departures from ideal aerodynamic performance. This concept is based on work of Reller (1957), who has pointed out that this shape results from a method of designing low heat transfer bodies. According to Reller (1957), low heat transfer bodies is devised on the premise that the rate of heat transfer to the nose will be low if the local velocity is low, while the rate of heat transfer to the afterbody will be low if the local density is low.

Santos (2003) has investigated the effect of the leading edge thickness on the aerodynamic surface quantities over these flat-nose leading edges. The thickness effect was examined for a range of Knudsen number, based on the thickness of the flat nose, covering from the transitional flow regime to the free molecular flow regime. The emphasis of the work was to compare the heat transfer and drag of this new shape with those obtained for round leading edge. It was found that flat-nose leading edges provided lower drag than round leading edge. Nevertheless, round leading edge yielded smaller stagnation point heating than the flat-nose leading edges for the conditions investigated.

Based on recent interest in hypersonic waveriders for high-altitude/low-density applications (Anderson, 1990, Potter and Rockaway, 1994, Rault, 1994, Graves and Argrow, 2001), this paper extends the analysis presented by Santos (2003) by investigating computationally the shock wave structure over these new contours. The primary goal is to assess the sensitivity of the shock standoff distance, shock wave thickness and shock wave shape to variations on the thickness of the leading edge and on the body surface temperature. Comparisons based on shock standoff distance are also made to examine the benefits and disadvantages of using these new blunt shapes over round shapes.

For the transitional hypersonic flow, at high Mach number and high altitude, the flow departs from thermal equilibrium and the energy exchange into the various modes due to the vibrational excitation and relaxation becomes important. For the high altitude/high Knudsen number of interest ($Kn > 0.1$), the flowfield is sufficiently rarefied that continuum method is inappropriate. In addition, the computational complexity and storage requirements associated with the Boltzmann equation (Cercignani, 1988) are prohibitive. Alternatively, the DSMC method is used in the current study to calculate the rarefied hypersonic two-dimensional flow on the leading edge shapes.

2. Body Shape Definition

In dimensionless form, the contour that defines the shape of the afterbody surface is given by,

$$\bar{x} = \int_{\bar{y}=1}^{\bar{y}=\bar{y}_{\max}} \sqrt{\bar{y}^k - 1}\, d\bar{y} \tag{1}$$

where $\bar{x} = x/y_{nose}$ and $\bar{y} = y/y_{nose}$ and k is a constant.

The blunt shapes are modeled by assuming a sharp leading edge of half angle θ with a circular cylinder of radius R inscribed tangent to the wedge. The blunt shapes, inscribed between the wedge and the cylinder, are also tangent to them at the same common point where they have the same slope angle. The circular cylinder diameter provides a reference for the amount of blunting desired on the leading edges. It was assumed a leading edge half angle of 10 deg, a circular cylinder diameter of 10^{-2}m and flat-nose thicknesses t/λ_∞ of 0.01, 0.1 and 1, where $t = 2y_{nose}$ and λ_∞ is the freestream mean free path. Figure (1a) illustrates this construction for the set of shapes investigated. From geometric considerations, the exponent k in Eq. (1) is obtained by matching slope on the wedge, circular cylinder and on the body shapes at the tangency point. For dimensionless thicknesses of 0.01, 0.1 and 1, the exponent k corresponds to 0.501, 0.746 and 1.465, respectively. The common body height H and the body length L are obtained in a straightforward manner. It was assumed that the leading edges are infinitely long but only the length L is considered, since the wake region behind the leading edges is not of interest in this investigation.

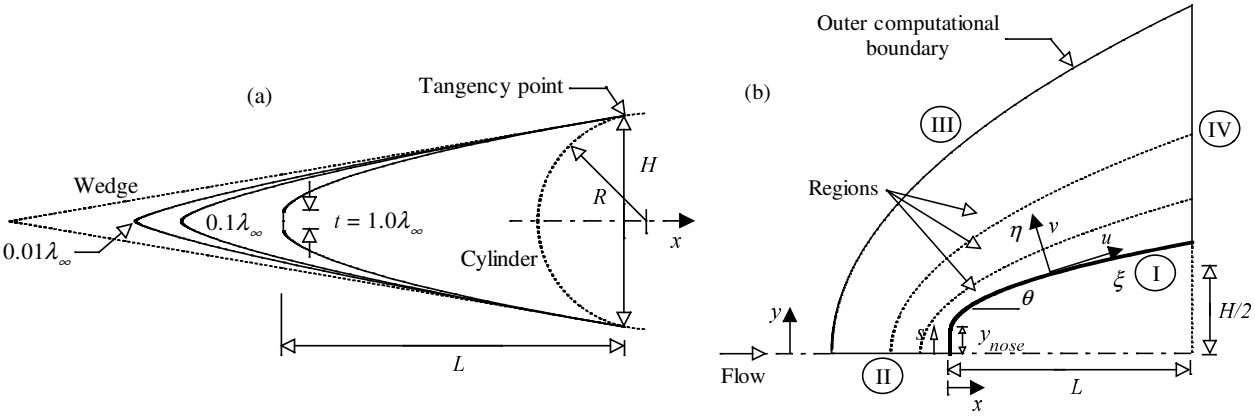

Figure 1: Drawing illustrating (a) the leading edge shapes and (b) the computational domain.

3. Computational Method

The Direct Simulation Monte Carlo (DSMC) method, pioneered by Bird (1994), has become one of the standard and reliable successful numerical techniques for modeling complex flows in the transition regime. The transition regime is the category of flow that falls between the continuum regime, where the Navier-Stokes equations are valid, and the free molecular regime, which is the limit of infinite Knudsen number.

In the DSMC method, a group of representative molecules are tracked as they move, collide and undergo boundary interactions in simulated physical space. Each simulated molecule represents a very much larger number of real molecules. The molecular motion, which is considered to be deterministic, and the intermolecular collisions, which are considered to be stochastic, are uncoupled over the small time step used to advance the simulation and computed sequentially. The simulation is always calculated as unsteady flow. However, a steady flow solution is obtained as the large time state of the simulation. In general, the total simulation time, discretized into time steps, is identified with the physical time of the real flow. Moreover, the time step should be chosen to be sufficiently small in comparison with the local mean collision time (Garcia and Wagner, 2000, and Hadjiconstantinou, 2000).

The molecular collisions are modeled using the variable hard sphere (VHS) molecular model (Bird, 1981) and the no time counter (NTC) collision sampling technique (Bird, 1989). The energy exchange between kinetic and internal modes is controlled by the Borgnakke-Larsen statistical model (Borgnakke and Larsen, 1975). Simulations are performed using a non-reacting gas model consisting of two chemical species, N_2 and O_2. Energy exchanges between the translational and internal modes are considered. For this study, the relaxation numbers of 5 and 50 were used for the rotation and vibration, respectively.

The flowfield is divided into a number of regions, which are subdivided into computational cells. The cells are further subdivided into four subcells, two subcells/cell in each coordinate direction. The cell provides a convenient reference for the sampling of the macroscopic gas properties, while the collision partners are selected from the same

subcell for the establishment of the collision rate. The linear dimensions of the cells should be small in comparison with the scale length of the macroscopic flow gradients normal to the streamwise directions, which means that the cell dimensions should be of the order of or even smaller than the local mean free path (Alexander et al., 1998 and Alexander et al., 2000).

The computational domain used for the calculation is made large enough so that body disturbances do not reach the upstream and side boundaries, where freestream conditions are specified. A schematic view of the computational domain is depicted in Fig. (1b). Side I is defined by the body surface. Diffuse reflection with complete thermal accommodation is the condition applied to this side. Advantage of the flow symmetry is taken into account, and molecular simulation is applied to one-half of a full configuration. Thus, side II is a plane of symmetry, where all flow gradients normal to the plane are zero. At the molecular level, this plane is equivalent to a specular reflecting boundary. Side III is the freestream side through which simulated molecules enter and exit. Finally, the flow at the downstream outflow boundary, side IV, is predominantly supersonic and vacuum condition is specified (Guo and Liaw, 2001). At this boundary, simulated molecules can only exit.

Numerical accuracy in DSMC method depends on the grid resolution chosen as well as the number of particles per computational cell. Both effects were investigated to determine the number of cells and the number of particles required to achieve grid independence solutions. Grid independence was tested by running the calculations with half and double the number of cells in ξ and η directions (see Fig. (1b)) compared to a standard grid. Solutions (not shown) were near identical for all grids used and were considered fully grid independent.

4. Freestream and Flow Conditions

The freestream and flow conditions used in the present calculations are those given by Santos (2003) and summarized in Tab. (1). The gas properties considered in the simulation are those given by Bird (1994) and shown in Tab. (2). The freestream velocity V_∞, assumed to be constant at 3.56 km/s, corresponds to a freestream Mach number M_∞ of 12. In order to simulate the surface temperature effects, the wall temperature T_w is assumed constant at 440, 660, 880 and 1100 K, which correspond to 2, 3, 4 and 5 times the freestream temperature, respectively.

Table 1: Freestream Conditions

Temperature T_∞ (K)	Pressure p_∞ (N/m^2)	Density ρ_∞ (kg/m^3)	Number density n_∞ (m^{-3})	Viscosity μ_∞ (Ns/m^2)	Mean free path λ_∞ (m)	Velocity V_∞ (m/s)
220.0	5.582	8.753×10^{-5}	1.8209×10^{21}	1.455×10^{-5}	9.03×10^{-4}	3560

Table 2: Gas Properties

	Mole fraction X	Molecular mass m (kg)	Molecular diameter d (m)	Viscosity Index ω
O_2	0.237	5.312×10^{-26}	4.01×10^{-10}	0.77
N_2	0.763	4.65×10^{-26}	4.11×10^{-10}	0.74

The overall Knudsen number Kn_t, defined as the ratio of the freestream mean free path λ_∞ to the leading edge thickness t, corresponds to 1, 10 and 100 for leading edge thicknesses t/λ_∞ of 1, 0.1 and 0.01, respectively. The Reynolds number Re_t covers the range from 0.193 to 19.3, based on conditions in the undisturbed stream with leading edge thickness t as the characteristic length.

5. Computational Procedure

The problem of predicting the shape and location of detached shock waves has been stimulated by the necessity for blunt noses and leading edges configurations designed for hypersonic flight in order to cope with the aerodynamic heating. In addition, the ability to predict the shape and location of shock waves is of primary importance in analysis of aerodynamic interference. Furthermore, the knowledge of the shock wave displacement is especially important in a waverider geometry (Nonweiler, 1959), since these hypersonic configurations usually rely on shock wave attachment at the leading edge to achieve their high lift-to-drag ratio at high-lift coefficient.

In this present account, the shock wave structure, defined by shape, thickness and detachment of the shock wave, is predicted by employing a procedure based on the physics of the particles. In this respect, the flow is assumed to consist of three distinct classes of molecules; those molecules from the freestream that have not been affected by the presence of the leading edge are denoted as class I molecules; those molecules that, at some time in their past history, have struck and been reflected from the body surface are denoted as class II molecules; and finally, those molecules that have been indirectly affected by the presence of the body are defined as class III molecules. Figure (2a) illustrates the definition for the molecular classes.

It is assumed that the class I molecule changes to class III molecule when it collides with class II or class III molecule. Class I or class III molecule is progressively transformed into class II molecule when it interacts with the body surface. Also, a class II molecule remains class II regardless of subsequent collisions and interactions. Hence, the transition from class I molecules to class III molecules may represent the shock wave, and the transition from class III to class II may define the boundary layer.

A typical distribution of class III molecules along the stagnation streamline for blunt leading edges is displayed in Fig. (2b) along with the definition used to determine the thickness, displacement and shape of the shock wave. In this figure, X is the distance x along the stagnation streamline (see Fig. (1b)), normalized by the freestream mean free path λ_∞, and f_{III} is the number of molecules for class III to the total amount of molecules inside each cell.

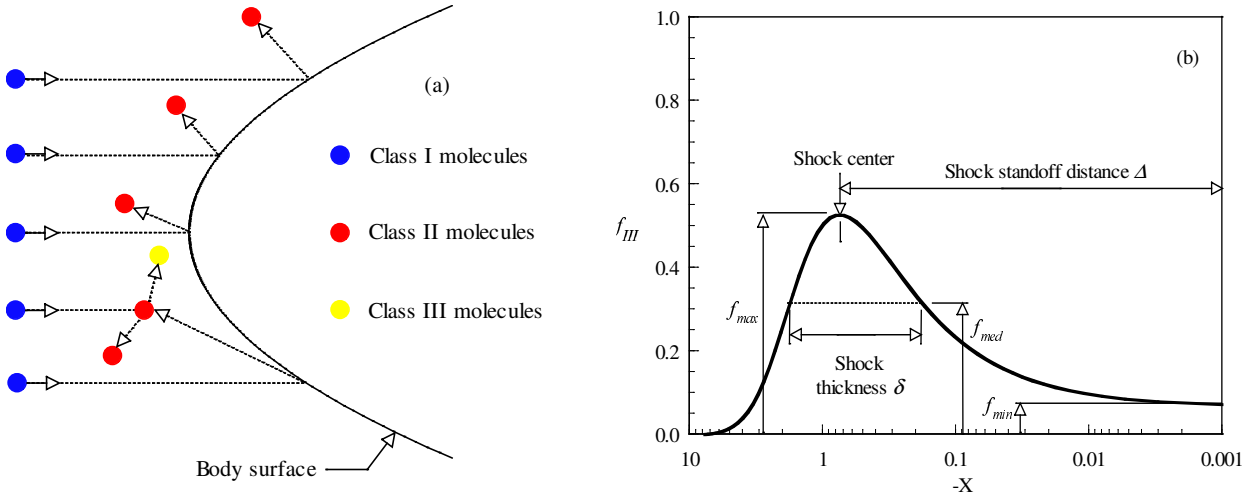

Figure 2: (a) Drawing illustrating the classification of molecules and (b) Schematic of shock wave structure.

In a rarefied flow, the shock wave has a finite region that depends on the transport properties of the gas, and can no longer be considered as a discontinuity obeying the classical Rankine-Hugoniot relations. In this context, the shock standoff distance Δ is defined as being the distance between the shock wave center and the nose of the leading edge along the stagnation streamline. As shown in Fig. (2b), the center of the shock wave is defined by the station that corresponds to the maximum value for f_{III}. The shock wave thickness δ is defined by the distance between the stations that correspond to the mean value for f_{III}. Finally, the shock wave shape (shock wave "location") is determined by the coordinate points given by the maximum value in the f_{III} distribution along the lines departing from the body surface, i.e., η-direction as shown in Fig. (1b).

The molecule classification that has been adopted here was first presented by Lubonski (1962) in order to study the hypervelocity Couette flow near the free molecule regime. Lubonski (1962) divided the gas into three classes of molecules: "freestream", "reflected from the boundary" and "scattered". Later, for the purpose of flow visualization, Bird (1969) applied the same scheme of classification by identifying the classes by colors: blue for class I, red for class II and yellow for class III molecules.

6. Computational Results and Discussions

The purpose of this section is to discuss and to compare differences in the shape, thickness and displacement of the shock wave due to variations on the body surface temperature as well as on the leading edge thickness.

The distribution of molecules for the three classes along the stagnation streamline is illustrated in Figs. (3) and (4) for four cases that combine two different nose thicknesses, Kn_t of 100 and 1 (t/λ_∞ of 0.01 and 1), and wall temperatures of 440 K and 1100 K. The class distributions for the other cases investigated in this work are intermediate to these four cases and, therefore, they will not be shown.

Referring to Figs. (3) and (4), f_I, f_{II} and f_{III} are the ratio of the number of molecules for class I, II and III, respectively, to the total amount of molecules inside each cell along the stagnation streamline. Of great significance in these figures is the behavior of the class I molecules for sharp and blunt leading edges. It should be observed that molecules from freestream, represented by class I molecules, collide with the nose of the leading edges even after the establishment of the steady state. This is shown in Fig. (3), which represent sharp leading edge cases. In contrast, molecules from freestream do not reach the nose of the leading edge for those cases illustrated in Fig. (4), that represent blunt leading edges. This is explained by the fact that density (Santos, 2004) increases much more for blunt (flat) leading edges in the stagnation region and reach its maximum value in the stagnation point. In this connection, the buildup of particle density near the nose of the leading edge acts as a shield for the molecules coming from the undisturbed stream.

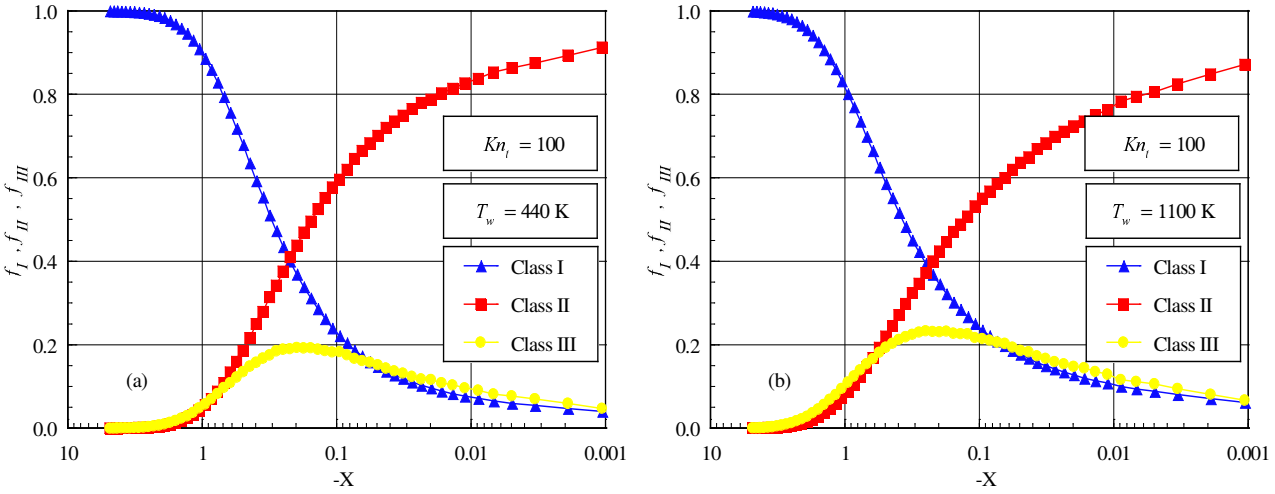

Figure 3: Distributions of molecules for classes I, II and III along the stagnation streamline for leading edge thickness that correspond to Knudsen number Kn_t of 100 and wall temperature of (a) 440 K and (b) 1100 K.

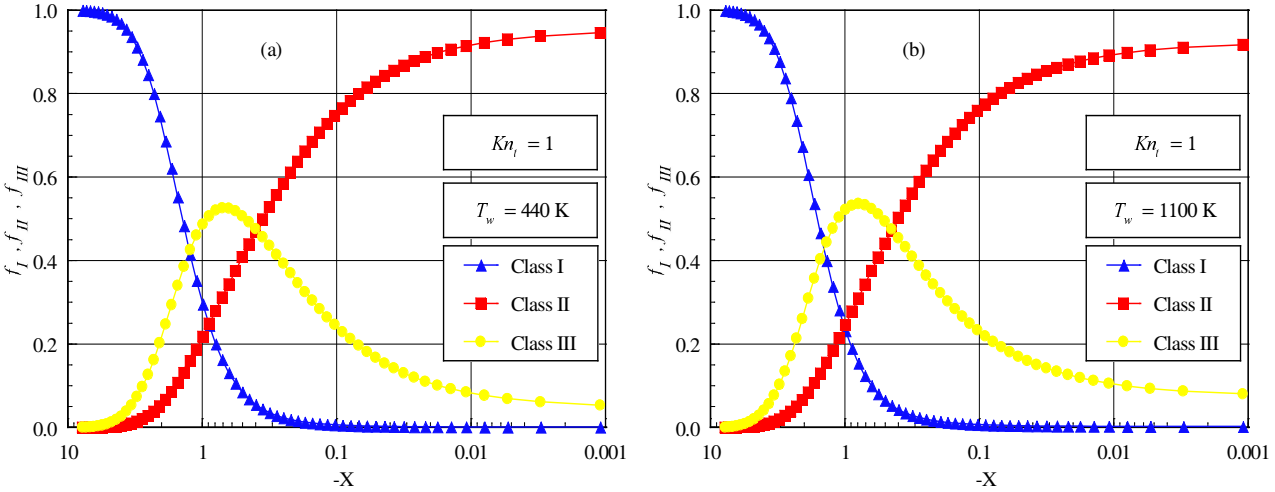

Figure 4: Distributions of molecules for classes I, II and III along the stagnation streamline for leading edge thickness that correspond to Knudsen number Kn_t of 1 and wall temperature of (a) 440 K and (b) 1100 K.

6.1. Shock Wave Standoff Distance

According to the definition shown in Fig. (2b), the shock wave standoff distance Δ can be observed in Figs. (3) and (4) for the flat-nose shapes shown. The calculated shock wave standoff distance Δ, normalized by the freestream mean free path λ_∞, is tabulated in Table (3) for the cases investigated. It is apparent from these results that there is a discrete shock standoff distance for the cases shown. As would be expected, the shock standoff distance increases with increasing the flat-nose thickness. Moreover, the shock standoff distance also increases with the wall temperature rise. As a reference, for wall temperature of 1100 K, the shock wave standoff distance for cases Kn_t of 100, 10 and 1 is around 1.2, 1.2 and 1.16 times, respectively, larger than those for wall temperature of 440 K.

Table 3: Dimensionless shock wave standoff distance Δ/λ_∞ for flat-nose leading edges.

T_w	$Kn_t = 100$	$Kn_t = 10$	$Kn_t = 1$
440 K	0.183	0.298	0.672
660 K	0.184	0.336	0.714
880 K	0.201	0.346	0.753
1100 K	0.218	0.357	0.781

For comparison purpose, the circular cylinder, shown in Fig. (1a), provides a larger shock detachment, i.e., Δ/λ_∞ of 1.645 for wall temperature of 880 K. This value is about 8.2, 4.8 and 2.2 times larger than the cases corresponding to Kn_t of 100, 10 and 1, respectively, for the same wall temperature. The results tend to confirm the expectation that the

shock standoff distance for sharp leading edge is smaller than that for blunt leading edge. In fact, the flat-nose bodies behave as if they had a sharper profile than the representative circular cylinder.

It is important to mention that shock standoff distance becomes important in hypersonic vehicles such as waveriders, which depend on leading edge shock attachment to achieve their high lift-to-drag ratio at high lift coefficient. In this connection, the flat-nose shapes seem to be more appropriate than the circular cylinder, since they present reduced shock wave detachment distances. Nonetheless, smaller shock detachment distance is associated with a higher heat load to the nose of the body. According to Santos (2003), the heat transfer coefficient C_{ho} (= $2q_w/\rho_\infty V_\infty^2$) at the stagnation point for flat-nose bodies, Kn_t of 100, 10 and 1, with temperature of 880 K, are 2.4, 2.2 and 1.5 times larger than the heat transfer coefficient for the circular cylinder at the same conditions. As a result, it should be notice from this comparison that the ideal blunting leading edge depends on the context. If shock standoff distance is the primary issue in leading edge design of hypersonic waveriders, then flat-nose leading edges are superior to round leading edges (circular cylinder). Contrary, if the stagnation point heating is the important parameter in the hypersonic vehicle design, then round shapes seem to be superior to the flat-nose shapes.

6.2. Shock Wave Thickness

Based on the definition of the shock wave thickness shown in Fig. (2b), the shock wave thickness δ along the stagnation streamline can be obtained from Figs. (3) and (4) for the flat-nose shapes. As a result of the calculation, Table (4) tabulates the shock wave thickness δ, normalized by the freestream mean free path λ_∞, for the cases investigated.

Table 4: Dimensionless shock wave thickness δ/λ_∞ for flat-nose leading edges.

T_w	$Kn_t = 100$	$Kn_t = 10$	$Kn_t = 1$
440 K	0.544	0.742	1.584
660 K	0.607	0.808	1.626
880 K	0.652	0.864	1.673
1100 K	0.693	0.907	1.715

The circular cylinder provides a much larger shock thickness, i.e., δ/λ_∞, of 3.350 for wall temperature of 880 K. Compared to the flat-nose shapes, this value is about 5.3, 3.9 and 2.0 times larger than the cases corresponding to Kn_t of 100, 10 and 1, respectively, with temperature of 880 K.

6.3. Shock Wave Shape

The shock wave shape, defined by the shock wave center location, is obtained by calculating the position that corresponds to the maximum f for class III molecules in the η-direction along the body surface (see Fig. (1b)). Figure (5) illustrates the shock wave shape in the vicinity of the stagnation region for cases Kn_t of 100 and 1, which correspond to flat-nose bodies with thicknesses t/λ_∞ of 0.01 and 1, respectively. Only shock wave shapes for cases with wall temperatures of 440 K and 1100 K were shown. The shock wave shape for the other cases (not shown) are intermediate to the cases depicted in Fig. (5). In this set of plots, X and Y are the Cartesian coordinates x and y normalized by λ_∞.

It was pointed out by Lees and Kubota (1957) that when the freestream Mach number M_∞ is sufficiently large, the hypersonic small-disturbance equations admit similarity solutions for the asymptotic shock wave shapes over power-law bodies ($y \propto x^n$, $0 < n < 1$), where asymptotic refers to the flowfield at large distances downstream of the nose of the body. The hypersonic small-disturbance theory states that, for certain exponent n, a body defined by x^n produces a shock wave of similar shape and profiles of flow properties transverse to the stream direction that are similar at any axial station not too near the nose. At or near the nose, the surface slope, the curvature, and the higher derivatives are infinite, and the similarity solutions break down. In the more general case for $0 < n < 1$, the shock wave grows as x^m. When n grows from zero, m begins by keeping the constant value $m = 2/(j+3)$, and if n keeps on growing towards unity, m remains equal to n. Here j takes the values zero for planar flow and one for axisymmetric flow.

The flat-nose bodies, defined by Eq.(1), are not power-law shapes themselves, by they can be closely fitted with power-law shapes ($\propto x^n$) far from the nose of the leading edge. Figure (6a) displays the comparison of the flat-nose shapes and the corresponding power-law curve fit shapes. As would be expected, discrepancies have been found among the curves in the vicinity of the nose of the bodies. This behavior is brought out more clearly in Fig. (6b), which exhibits details of the curves near the nose.

By considering the reference system located at the nose of the flat-nose bodies, $X = 0$, the fitting process, which has been performed over those bodies shown in Fig. (6), approximates the body shapes by power-law shape of the following form,

$$y = a(x+b)^n \tag{2}$$

where a is the power-law constant of the curve fit, b is the distance from the nose of the leading edge, and n is the power law exponent of the curve fit. The coefficients a and b, normalized, respectively, by $\lambda_\infty^{(1-n)}$ and λ_∞, and the exponent n are tabulated in Table (5). The maximum absolute error between the original shapes and the curve fit shapes for $X > 3$ are less than 0.12%, 0.14% and 0.30% for flat-nose thicknesses corresponding to Kn_t of 100, 10 and 1, respectively.

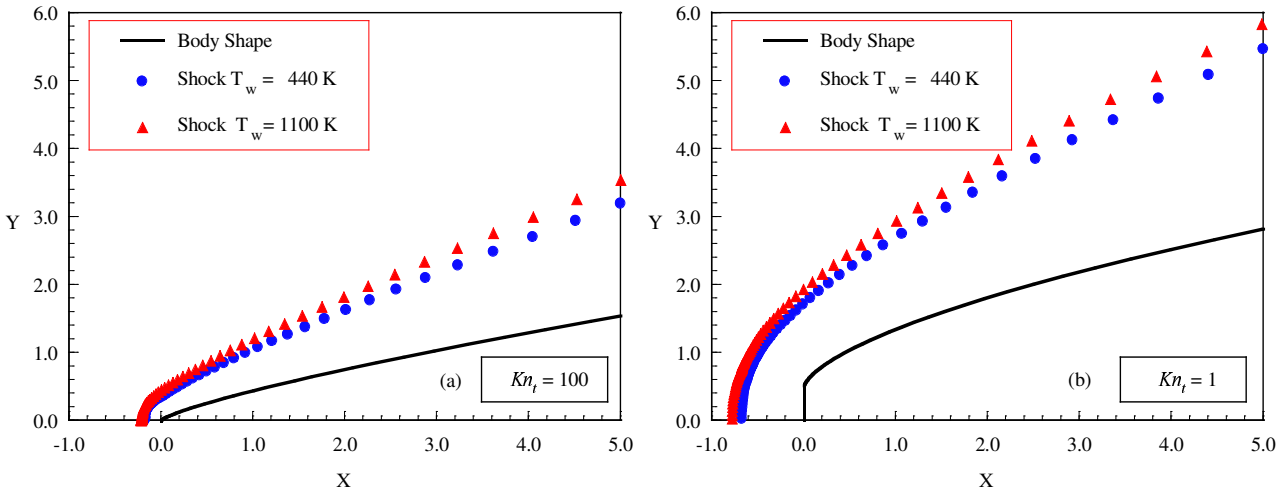

Figure 5: Shock wave shapes on flat-nose bodies as a function of the wall temperature for leading edge thicknesses that correspond to Knudsen number Kn_t of (a) 100 and (b) 1.

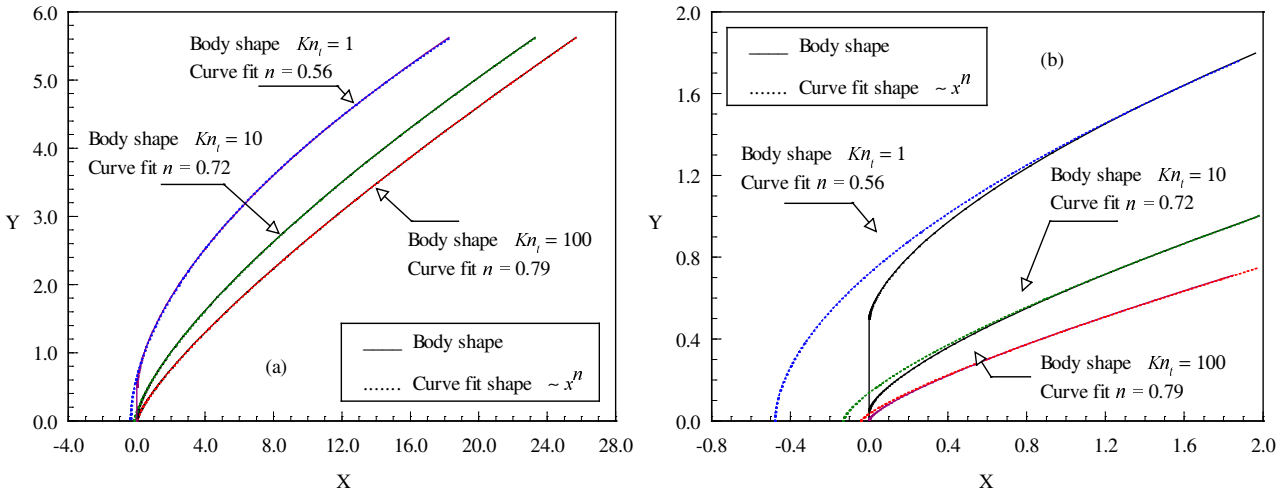

Figure 6: Comparison of flat-nose shapes with power-law curve fit shapes for leading edge thicknesses t/λ_∞ of 0.01, 0.1 and 1, which correspond to Knudsen number Kn_t 100, 10 and 1. (a) along the afterbody surface and (b) in the vicinity of the nose.

Table 5: Dimensionless coefficients a, b, and n for the curve fit power law bodies.

Kn_t	a	b	n
100	0.42893	0.04120	0.79
10	0.58436	0.13318	0.72
1	1.09002	0.47817	0.56

In what follows, the flat-nose leading edges shown in Fig. (6) are now well represented by shapes with the power-law form ($\propto x^n$) far from the nose of the leading edges. Hence, by assuming that power-law bodies generate power-law shock waves in accordance with hypersonic small-disturbance theory (Lees and Kubota, 1957), the shock location coordinates shown in Fig. (5) were used to approximate the shape of the shock wave with a curve fit. A fitting algorithm was performed over these points to approximate the shock shape as a power law curve of the following form,

$$y = A(x + B)^m \tag{3}$$

where A is the shock wave power law constant, B is the distance from the nose of the leading edge to the shock wave curve fit along the stagnation streamline, and m is the shock wave power law exponent.

For comparison purpose, two forms of the curve fit were considered in defining the shock shape: (1) A, B and m were found to provide the best curve fit solutions, and (2) A and B were found by keeping $m = 2/3$ for $n < 2/3$ cases, and $m = n$ for $n \geq 2/3$ cases, where n and m stand for body and shock wave power law exponents, respectively.

It is worthwhile mentioning that the fitting process was performed over the points yielded by DSMC simulations located far from the nose region, say $X > 3.0$, where it is expected that the blunt nose effects are not significant. It is also important to recall that the shock wave shape in the vicinity of the nose is not correctly predicted by the theoretical solutions, since the hypersonic slender body approximations are violated close to or at the nose of the leading edges as explained above. Moreover, the flat-nose shapes are represented by power-law shapes far from the nose region, as displayed in Fig. (6).

Curve fit solutions for shock shape over the flat-nose body with Kn_t of 100 ($t/\lambda_\infty = 0.01$), which corresponds to a body power law exponent of 0.79, are displayed in Figs. (7a) and (7b) for wall temperature of 440 K and 1100 K, respectively. In Fig. (7a) (or (7b)), the solutions given by $m = 0.84$ (or $m = 0.82$) and $m = n = 0.79$ represent, respectively, the two forms of the curve fit solutions mentioned above. It is apparent from this set of figures that the curve fit solutions present a good agreement, by visual inspection, with those solutions provided by the DSMC simulation. Nevertheless, as the maximum absolute error between the DSMC solutions and the curve fit solutions are calculated for coordinate points located at $X > 3.0$, it is found that the best fit is obtained for the first form of the fitting process, i.e., when A, B and m were found in order to yield the best solution. The error is less then 1.0% and 1.4% for $m = 0.84$ or 0.82 and 0.79, respectively, for the curves in Fig. (7a) and (7b). In general, the solutions are in qualitative agreement with the Lees and Kubota (1957) findings in the sense that the shock wave shape would follow the shape of the body for body power law exponent $n > 2/3$.

Shock shape curve fit solutions for the flat-nose body with Kn_t of 1 ($t/\lambda_\infty = 1$), which corresponds to a body power law exponent of 0.56, are displayed in Figs. (8a) and (8b) for body surface temperature of 440 K and 1100 K, respectively. The curve fit solutions shown in this set of figures were obtained according to Eq.(3) by three different forms; in the first form, A and B were found by keeping m equal to the body shape, $m = n$; in the second form, A, B and m were found in order to obtain the best fit; finally in the third form, A and B were found by keeping m equal to 2/3, the exponent that it is expected that the shock wave would grow, according to the theory (Lees and Kubota, 1957).

Referring to Figs. (8a) and (8b), it is noted that the curve fit given by $m = n = 0.56$ does not match the shock wave shape obtained by the DSMC simulation, as predicted by the hypersonic small-disturbance theory (Lees and Kubota, 1957). In contrast, the two other curve fit solutions, m equal to 2/3, 0.71 in Fig. (8a) and 0.70 in Fig.(8b) present an excellent agreement with those solutions provided by the DSMC simulation. Once again, the curve-fitted solution deviates from the DSMC solution close to the nose of the leading edge, as would be expected.

At this point, it should be emphasized that the curve fit exponents are very sensitive to the number of coordinate points, which define the shock wave, used in the fitting process. In addition, these coordinate points present fluctuations, originated from the DSMC simulations, which were not taken into account.

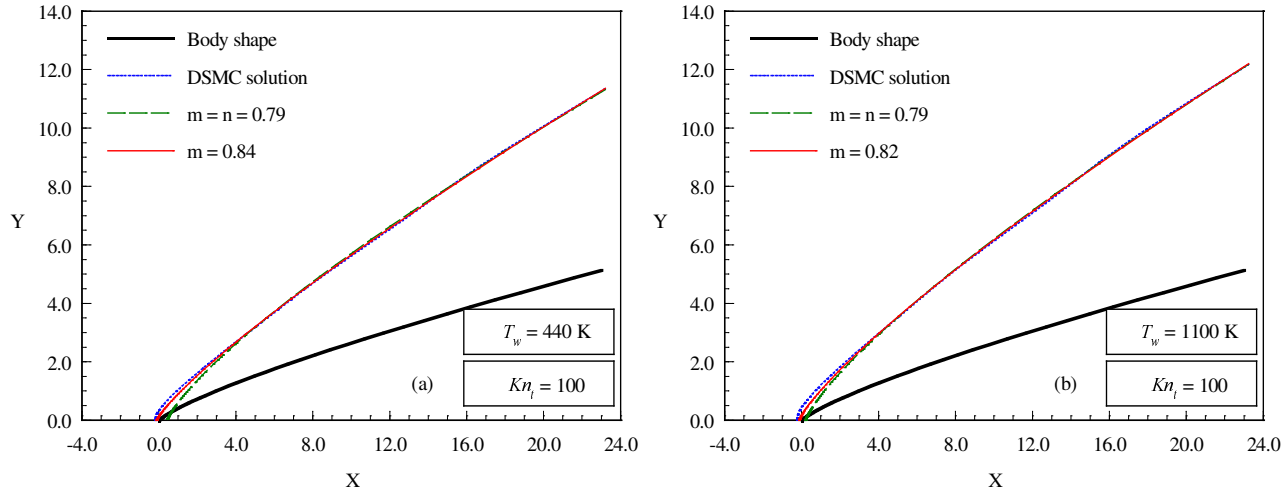

Figure 7: Shock wave shape curve fits on flat-nose body with thicknesses t/λ_∞ of 0.01, which corresponds to Knudsen number Kn_t 100. For wall temperatures of (a) 440 K and (b) 1100 K.

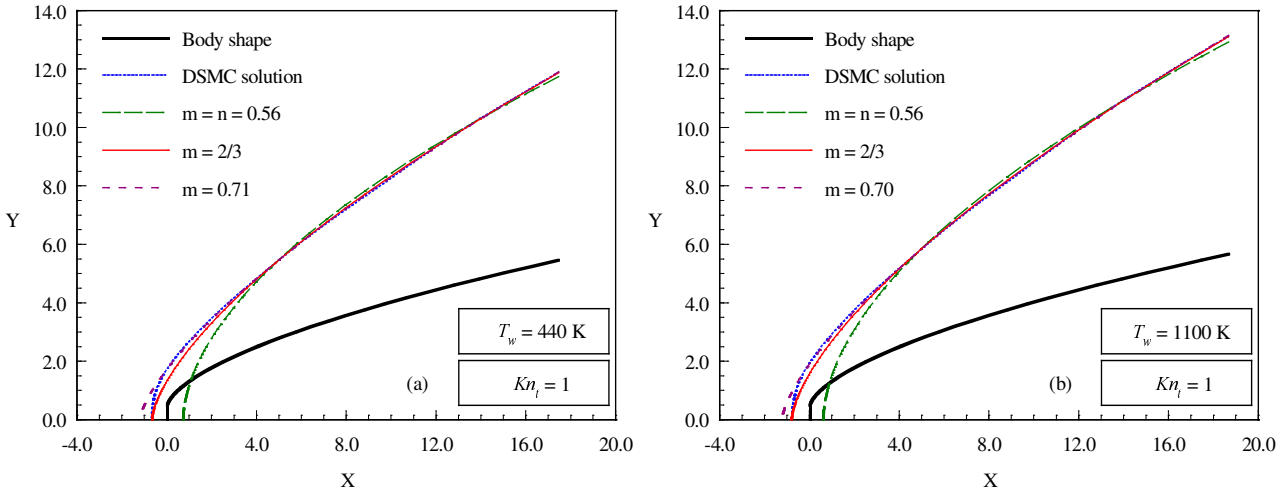

Figure 8: Shock wave shape curve fits on flat-nose body with thicknesses t/λ_∞ of 1, which corresponds to Knudsen number Kn_t 1. For wall temperatures of (a) 440 K and (b) 1100 K.

Finally, for comparison purpose, the coefficients A and B, normalized, respectively, by $\lambda_\infty^{(1-m)}$ and λ_∞, and the exponent m are tabulated in Table. (6).

Table 6: Dimensionless coefficients A, B, and m for the curve fit power law bodies.

T_w	Kn_t	A	B	m
440 K	100	0.95755	- 0.43187	0.79
	100	0.81664	0.11801	0.84
1100 K	100	1.02157	- 0.20607	0.79
	100	0.93108	0.12246	0.82
440 K	1	2.42593	- 0.71967	0.56
	1	1.71967	0.66279	2/3
	1	1.50197	1.21651	0.71
1100 K	1	2.55882	- 0.60505	0.56
	1	1.81104	0.80247	2/3
	1	1.62838	1.24265	0.70

7. Concluding Remarks

This study applies the Direct Simulation Monte Carlo method to investigate the shock wave structure for a family of flat-nose leading edges. The calculations have provided information concerning the nature of the shock wave detachment distance, shock wave thickness and shock wave shape resulting from variations on the thickness of the flat nose and on the body surface temperature for the idealized situation of two-dimensional hypersonic rarefied flow. The emphasis of the investigation was also to compare these flat-nose leading edges with round shape (circular cylinder) in order to determine which geometry is better suited as a blunting profiles in terms of the shock wave standoff distance.

The analysis showed that the shock wave structure was affected by changes in the wall temperature. It was found that the shock wave standoff and the shock wave thickness increased with the wall temperature rise for the range of wall temperature investigated. In addition, the shock wave was displaced further upstream the nose of the leading edges with increasing the wall temperature. It was also found that the shock wave standoff distance and the shock wave thickness for the flat-nose bodies are lower than that for the circular body with the same tangency to a wedge of specified oblique angle. In addition, the computational results indicated that the shock wave shape grows with power law form ($\propto x^m$), for the flat-nose bodies investigated, which can be closely fitted with power-law shapes ($\propto x^n$).

8. References

Alexander, F. J., Garcia, A. L., and, Alder, B. J., 1998, "Cell Size Dependence of Transport Coefficient in Stochastic Particle Algorithms", Physics of Fluids, Vol. 10, No. 6, pp. 1540-1542.

Alexander, F. J., Garcia, A. L., and, Alder, B. J., 2000, "Erratum: Cell Size Dependence of Transport Coefficient is Stochastic Particle Algorithms", Physics of Fluids, Vol. 12, No. 3, pp. 731-731.

Anderson, J. L., 1990, "Tethered Aerothermodynamic Research for Hypersonic Waveriders", Proceedings of the 1st International Hypersonic Waverider Symposium, Univ. of Maryland, College Park, MD.

Bird, G. A., 1969, "The Structure of Rarefied Gas Flows Past Simple Aerodynamic Shapes", Journal of Fluid Mechanics, Vol. 36, No. 3, pp. 571-576.

Bird, G. A., 1981, "Monte Carlo Simulation in an Engineering Context", Progress in Astronautics and Aeronautics: Rarefied gas Dynamics, Ed. Sam S. Fisher, Vol. 74, part I, AIAA New York, pp. 239-255.

Bird, G. A., 1989, "Perception of Numerical Method in Rarefied Gasdynamics", Rarefied gas Dynamics: Theoretical and Computational Techniques, Eds. E. P. Muntz, and D. P. Weaver and D. H. Capbell, Vol. 118, Progress in Astronautics and Aeronautics, AIAA, New York, pp. 374-395.

Bird, G. A., 1994, "Molecular Gas Dynamics and the Direct Simulation of Gas Flows", Oxford University Press, Oxford, England, UK.

Borgnakke, C. and Larsen, P. S., 1975, "Statistical Collision Model for Monte Carlo Simulation of Polyatomic Gas Mixture", Journal of computational Physics, Vol. 18, No. 4, pp. 405-420.

Cercignani, C., 1988, "The Boltzmann Equation and Its Applications", Springer-Verlag, New York, NY.

Garcia, A. L., and, Wagner, W., 2000, "Time Step Truncation Error in Direct Simulation Monte Carlo", Physics of Fluids, Vol. 12, No. 10, 2000, pp. 2621-2633.

Graves, R. E. and Argrow, B. M., 2001, "Aerodynamic Performance of an Osculating-Cones Waverider at High Altitudes", 35th AIAA Thermophysics Conference, AIAA Paper 2001-2960, Anaheim, CA.

Guo, K. and Liaw, G.-S., 2001, "A Review: Boundary Conditions for the DSMC Method", Proceedings of the 35th AIAA Thermophysics Conference, AIAA Paper 2001-2953, Anaheim, CA, 11-14 June.

Hadjiconstantinou, N. G., 2000, "Analysis of Discretization in the Direct Simulation Monte Carlo", Physics of Fluids, Vol. 12, No. 10, pp. 2634-2638.

Lees, L. and Kubota, T., 1957, "Inviscid Hypersonic Flow over Blunt-Nosed Slender Bodies", Journal of Aeronautical Sciences, Vol. 24, No. 3, pp. 195-202.

Lubonski, J., 1962, "Hypersonic Plane Couette Flow in Rarefied Gas", Archiwum Mechaniki Stosowanej, Vol. 14, No. 3/4, pp. 553-560.

Nonweiler, T. R. F., 1959, "Aerodynamic Problems of Manned Space Vehicles", Journal of the Royal Aeronautical Society, Vol. 63, Sept, pp. 521-528.

Potter, J. L. and Rockaway, J. K., 1994, "Aerodynamic Optimization for Hypersonic Flight at Very High Altitudes", Rarefied gas Dynamics: Space Science and Engineering, edited by B. D. Shizgal and D. P. Weaver, Vol. 160, Progress in Astronautics and Aeronautics, AIAA New York, pp. 296-307.

Rault, D. F. G., 1994, "Aerodynamic Characteristics of a Hypersonic Viscous Optimized Waverider at High Altitude", Journal of Spacecraft and Rockets, Vol. 31, No. 5, pp. 719-727.

Reller Jr., J. O., 1957, "Heat Transfer to Blunt Nose Shapes with Laminar Boundary Layers at High Supersonic Speeds", NACA RM-A57FO3a.

Santos, W. F. N., 2003, "Aerodynamic Heating on Blunt Nose Shapes in Rarefied Hypersonic Flow", Proceedings of the 17th International Congress of Mechanical Engineering COBEM 2003, 10-14 Nov, São Paulo, SP, Brazil.

Santos, W. F. N., 2004, "Surface Temperature Effects in Low-Density Flow over Flat-Nose Bodies at Hypersonic Speed. Part I: Flowfield Structure", Proceedings of the 10th Brazilian Congress of Thermal Sciences and Engineering ENCIT 2004, 29 Nov - 3 Dec, Rio de Janeiro, RJ, Brazil.